

Quantile motion of electromagnetic waves in wave guides of varying cross section and dispersive media

H.D. Dahmen, E. Gjonaj, T. Stroh
Fachbereich Physik, Universität Siegen, 57068 Siegen, Germany
 (August 24, 2018)

We discuss applications of the quantile concept of trajectories and velocities to the propagation of electromagnetic signals in wave guides of varying cross section. Quantile motion is a general description of the transport properties of measurable conserved quantities in quantum mechanics as well as in classical electrodynamics. In the latter case we consider the quantile motion of electromagnetic energy as the direct result of a physical measurement. In this sense the quantile velocity corresponds to the electromagnetic signal velocity also in the presence of barriers and inhomogeneities in the medium of propagation. We show that this signal velocity is always smaller than the speed of light in vacuum. Using numerical examples we demonstrate how typical wave phenomena can be described in terms of the quantile motion.

I. INTRODUCTION

In recent years the tunneling of an evanescent electromagnetic pulse in a wave guide with a cross section reduced over part of the longitudinal extension of the wave guide has been studied. A series of microwave experiments [1–4] claims to have found superluminal tunneling velocities. The velocity of the signal has been identified with the velocity of the maximum of the pulse.

A physical detector always needs a certain amount of energy to change its state, therefore we use the quantile velocity of a density obtained by way of normalizing the electromagnetic energy density of the pulse to unity [5–7].

A numerical simulation of the microwave experiments with wave packets in wave guides with varying cross section is carried through. The quantile velocity of wave packets is studied numerically. It is shown rigorously that the quantile velocity is not superluminal. A short discussion of the quantile velocity in dispersive and absorptive media is presented. For a critical discussion of superluminal velocities of electromagnetic signals see also P. Thoma et al. [8], G. Raithel [9], G. Diener [10], and the contribution of H. Goenner in this workshop [11].

II. STATIONARY WAVES IN WAVE GUIDES OF VARYING CROSS SECTIONS. UNITARITY RELATIONS

We shall consider a wave guide of rectangular cross section and perfectly conducting walls, extending in the longitudinal z direction from $-\infty$ to $+\infty$. The simplest construction allowing an interpretation in terms of tunneling for an electromagnetic signal propagating in the wave guide is obtained by assuming a narrowing of the cross section, e.g., in the transverse x direction extending to the left of the origin for $z > 0$ as shown in Fig. VI. An electromagnetic wave moving from the right towards the narrowing of the cross section will be affected in a similar way as the quantum-mechanical wave function of a particle incident onto a potential step at $z = 0$.

To further simplify the problem we consider only the propagation of TE -waves of the type \mathbf{H}_{n0} for $n = 1, 2, \dots$. Such a situation can indeed be realized if we choose a constant height of the wave guide (b in Fig. VI) small enough for all waves of the type \mathbf{H}_{nm} with $m \geq 1$ to be evanescent [12]. Thus, the stationary electromagnetic field in the wave guide reduces to three field components, E_y , H_x , and H_z , each depending on x and z . One of the field components can be considered as independent, e.g., E_y , whereas the other two follow from the Maxwell equations, e.g., $i\omega\mu\mu_0\mathbf{H} = \nabla \times \mathbf{E}$, where ω is the frequency of the wave and $\mu = 1$ is the magnetic permeability of vacuum. It is worth noting that according to a well-known result [13,14] the magnetic field components are singular at the sharp edge of the narrowing. This implies an increase of the magnetic energy at the cost of the electric energy in the wave guide [12,14].

The solution for the stationary electric field component E_y fulfilling the Helmholtz wave equation with the appropriate boundary conditions is a superposition of modes

$$E_y^{n0}(x, z) = \begin{cases} \sin\left(\frac{n\pi x}{a}\right)e^{\pm i\kappa_n z}, & z < 0, \\ \sin\left(\frac{n\pi x}{a'}\right)e^{\pm i\kappa'_n z}, & z > 0, \end{cases} \quad (1)$$

where we denote $\kappa_n = \sqrt{(\omega/c)^2 - (n\pi/a)^2}$ and $\kappa'_n = \sqrt{(\omega/c)^2 - (n\pi/a')^2}$ the discrete wave numbers associated with the two regions of the wave guide. Considering a given mode \mathbf{H}_{m0} as the incoming wave incident from the right ($z < 0$) we are led to the ansatz for the solution

$$E_y(x, z) = \begin{cases} \sin(\frac{m\pi x}{a})e^{i\kappa_m z} + \sum_{n=1}^{\infty} \mathcal{A}_n^R \sin(\frac{n\pi x}{a})e^{-i\kappa_n z} \\ \sum_{n=1}^{\infty} \mathcal{A}_n^T \sin(\frac{n\pi x}{a'})e^{i\kappa'_n z} \end{cases} \quad (2)$$

for $z < 0$ and $z > 0$, respectively. Here, \mathcal{A}_n^R and \mathcal{A}_n^T are the (complex) amplitudes of the reflected and transmitted modes in complete analogy to the one-dimensional tunneling in quantum mechanics. However, an infinite number of different modes is needed in order to fulfill the boundary conditions at $z = 0$, so that the type of the outgoing wave does not necessarily coincide with that of the incoming wave.

Requiring continuity for the electric field component E_y at the wave-guide aperture at $z = 0$, we obtain for the amplitudes \mathcal{A}_n^R and \mathcal{A}_n^T

$$\begin{cases} \delta_{mn} + \mathcal{A}_n^R = \frac{2}{a} \int_0^{a'} dx \epsilon(x) \sin(\frac{n\pi x}{a}), \\ \mathcal{A}_n^T = \frac{2}{a'} \int_0^{a'} dx \epsilon(x) \sin(\frac{n\pi x}{a'}), \end{cases} \quad (3)$$

where $n = 1, 2, \dots$ and $\epsilon(x) = E_y(x, z = 0)$ is the value of the electric field strength at the aperture. Denoting $\delta_{mn} + \mathcal{A}_n^R \equiv \mathcal{A}_n^{(1)}$ and $\mathcal{A}_n^T \equiv \mathcal{A}_n^{(2)}$ we can equivalently write equations (3) as

$$\mathcal{A}_n^{(1)} = \frac{2}{a} \sum_{k=1}^{\infty} \Lambda_{nk} \mathcal{A}_k^{(2)}, \quad (4)$$

where

$$\Lambda_{nk} = (-1)^k \frac{a'k}{\pi} \frac{\sin(n\pi a'/a)}{(na'/a)^2 - k^2}.$$

The continuity condition for the transverse magnetic field component at $z = 0$ yields

$$\begin{aligned} \sum_{n=1}^{\infty} \kappa'_n \mathcal{A}_n^{(2)} \sin(\frac{n\pi x}{a'}) &= 2\kappa_m \sin(\frac{m\pi x}{a}) \\ - \sum_{n=1}^{\infty} \kappa_n \mathcal{A}_n^{(1)} \sin(\frac{n\pi x}{a}). \end{aligned} \quad (5)$$

Introducing equations (3) into (5) we obtain for the electric field $\epsilon(x)$ at the aperture the integral equation

$$\int_0^{a'} dx' \mathcal{K}(x, x') \epsilon(x') = \kappa_m \sin(\frac{m\pi x}{a}) \quad (6)$$

for $0 \leq x \leq a$. The kernel $\mathcal{K}(x, x')$ is given by

$$\begin{aligned} \mathcal{K}(x, x') &= \sum_{n=1}^{\infty} \left[\frac{\kappa_n}{a} \sin(\frac{n\pi x}{a}) \sin(\frac{n\pi x'}{a}) \right. \\ &\quad \left. + \frac{\kappa'_n}{a'} \sin(\frac{n\pi x}{a'}) \sin(\frac{n\pi x'}{a'}) \right]. \end{aligned} \quad (7)$$

The reflection and transmission amplitudes \mathcal{A}_n^R and \mathcal{A}_n^T follow then from the equations (3) and the solution of the integral equation (6).

In general the integral equation (6) is not solvable in closed form and the field $\epsilon(x)$ has to be determined numerically. We can, however, try to find approximate expressions for \mathcal{A}_n^R and \mathcal{A}_n^T by using the alternative representation of the integral equation (6) as a system of linear equations for the coefficients $\mathcal{A}_n^{(2)}$,

$$\sum_{n=1}^{\infty} \left[\delta_{nk} + \frac{4}{aa'\kappa'_k} T_{nk} \right] \mathcal{A}_n^{(2)} = \frac{4\kappa_m}{a'\kappa'_k} \Lambda_{mk} \quad (8)$$

with $k = 1, 2, \dots$ and matrix elements T_{nk} given by

$$T_{nk} = \sum_{l=1}^{\infty} \kappa_l \Lambda_{ln} \Lambda_{lk}. \quad (9)$$

Under certain conditions discussed below we can assume the matrix \mathbf{T} to be nearly diagonal and put its elements in the form

$$T_{nk} = \kappa'_k \left(\frac{a'}{2}\right)^2 (\delta_{nk} + m_{nk}), \quad (10)$$

where \mathbf{m} is a complex matrix with elements fulfilling $|m_{nk}| \ll 1$ for $n, k = 1, 2, \dots$. The solution of (8) follows then from the expansion of the corresponding inverse matrix into a fast converging Neumann series

$$\mathcal{A}_n^{(2)} = \frac{4\kappa_m}{a'} \left(\frac{a}{a+a'}\right) \sum_{k=1}^{\infty} \left[\mathbf{1} - \left(\frac{a'}{a+a'}\right) \mathbf{m} + \dots \right]_{nk} \frac{\Lambda_{mk}}{\kappa'_k}. \quad (11)$$

Neglecting all the terms in (11) but the leading one we obtain the coefficients

$$\mathcal{A}_n^{(2)} = (-1)^n \left(\frac{a}{a+a'}\right) \frac{4n\kappa_m}{\pi\kappa'_n} \frac{\sin(m\pi a'/a)}{(ma'/a)^2 - n^2} \quad (12)$$

for $n = 1, 2, \dots$, implying at $z = 0$ a transverse magnetic field component H_x given by

$$H_x(x, 0) = -\left(\frac{2a}{a+a'}\right) \frac{\kappa_m}{\omega\mu\mu_0} \sin(\frac{m\pi x}{a}). \quad (13)$$

Equation (13) predicts the increase in the magnitude of the transverse magnetic field component H_x at $z = 0$, whereas the shape of the field there obviously coincides with that of the incoming mode \mathbf{H}_{m0} . Thus, the approximation leading to (12) seems appropriate in the limiting case of geometric optics, i.e., if the wave length of the incoming wave is short compared to the cross sections a and a' of the wave guide. In the case of an evanescent wave for $z > 0$, however, more terms in the expansion (11) are needed for the boundary conditions at $z = 0$ to be fulfilled. Therefore, a numerical solution of equation (6) is used in what follows.

We now turn to a more complicated geometry for the wave guide involving two boundary conditions at $z = 0$ and $z = L$, where L is the length of a symmetrically

placed barrier (reduction of the cross section as shown in Fig. VI). Numerical simulations for the stationary field components in the wave guide are shown in Fig. VI and Fig. 4. The continuity of the transverse field components at the wave-guide aperture as well as the magnetic-field singularities at the narrowing edges are shown in Fig. VI. Figure 4 is a spectral diagram with reflection and transmission coefficients (in the regions $z < 0$ and $z > L$, respectively) of the incoming as well as of higher modes.

Because of the magnetic-field singularities in a real experiment the maxima of the magnetic field strength would always be located in the vicinity of the wave-guide edges. Therefore, they give no information on the velocity of a tunneling electromagnetic signal. If, instead, we refer to the electromagnetic energy density in the wave guide we can avoid dealing with singularities by recalling that the singularities of the energy density are integrable. Poynting's theorem in our case reads

$$\frac{\partial w_{\text{em}}(x, z, t)}{\partial t} + \frac{\partial s_x(x, z, t)}{\partial x} + \frac{\partial s_z(x, z, t)}{\partial z} = 0, \quad (14)$$

where w_{em} is the two-dimensional energy density and s_x and s_z are the components of the Poynting vector. Integrating (14) over the transverse direction x the second term in (14) vanishes and we obtain

$$\frac{\partial}{\partial t} \mathcal{W}(z, t) + \frac{\partial}{\partial z} \mathcal{S}_z(z, t) = 0, \quad (15)$$

where $\mathcal{W}(z, t)$ and $\mathcal{S}_z(z, t)$ are now the one-dimensional energy and current densities in the longitudinal direction z . These quantities are free of singularities and fulfill the one-dimensional continuity equation (15) in complete analogy to the probability and current density in the one-dimensional tunneling in quantum mechanics [15]. Therefore, it is appropriate to consider the energy density $\mathcal{W}(z, t)$ instead of the electric and magnetic field strengths in order to investigate the tunneling properties of electromagnetic signals in wave guides.

Returning to the stationary fields, we may use (15) to obtain unitarity relations between the reflection and transmission coefficients of the modes \mathcal{A}_n^{R} and \mathcal{A}_n^{T} , $n = 1, 2, \dots$. We find the time-averaged longitudinal current

$$\tilde{\mathcal{S}}_z(z) = -\frac{1}{2} \text{Re} \int dx E_y(x, z) H_x^*(x, z) \quad (16)$$

to be a constant along the wave guide. Comparing the expressions for $\tilde{\mathcal{S}}_z(z)$ in the reflection and transmission region we obtain

$$\sum_{n=1}^{n_c} \frac{\kappa_n}{\kappa_m} |\mathcal{A}_n^{\text{R}}|^2 + \frac{a'}{a} \sum_{n=1}^{n'_c} \frac{\kappa'_n}{\kappa_m} |\mathcal{A}_n^{\text{T}}|^2 = 1, \quad (17)$$

where $\mathbf{H}_{m,0}$ is the incoming mode, $\mathbf{H}_{n_c,0}$ and $\mathbf{H}_{n'_c,0}$ are the cutoff modes in the reflection and transmission region, respectively. The appearance in (17) of the upper limits

n_c and n'_c in the summation index n is a consequence of time averaging the current density $\mathcal{S}_z(z)$. Thus, equation (17) does not imply that only propagating modes $n \leq n_c$ ($n \leq n'_c$) are responsible for the energy transport through the barrier. In the microwave experiments [1–4] the cross sections a and a' of the reflection and transmission region were the same. With this assumption equation (17) reads

$$\sum_{n=1}^{n_c} \frac{\kappa_n}{\kappa_m} (|\mathcal{A}_n^{\text{R}}|^2 + |\mathcal{A}_n^{\text{T}}|^2) = 1. \quad (18)$$

Further simplifying the situation by allowing the ground mode \mathbf{H}_{10} as the only propagating mode in the wave guide yields the unitarity relation of the form

$$|\mathcal{A}_1^{\text{R}}|^2 + |\mathcal{A}_1^{\text{T}}|^2 = 1 \quad (19)$$

which clearly coincides with the corresponding equation in the one-dimensional quantum-mechanical tunneling.

III. TUNNELING OF WAVE PACKETS. COMPARISON WITH EXPERIMENTS

In the following we construct tunneling wave packets in the wave guide as a superposition of the stationary solutions found above. For such a superposition to be a propagating, incoming wave in the region to the right of the barrier ($z < 0$) it must not contain wave components below the cutoff frequency ω_c (evanescent components) in this region. Therefore we use, e.g., for the electric field component E_y the expression

$$E_y(x, z, t) = \int_{\omega_c}^{\infty} d\omega f(\omega) E_{ys}(x, z; \omega) e^{-i\omega t}, \quad (20)$$

where $f(\omega)$ is the spectral distribution of frequencies normalized in the interval (ω_c, ∞) and E_{ys} is the stationary electric field component.

In Fig. 5–Fig. 7 numerical simulations with Gaussian-like wave packets in the wave guide are shown. The spectral distribution $f(\omega)$ in this case is given by

$$f(\omega) = \frac{1}{\tilde{N}} \frac{\Theta(\omega - \omega_c)}{(\sqrt{2\pi}\sigma_\omega)^{1/2}} \exp\left(-\frac{(\omega - \omega_0)^2}{4\sigma_\omega^2}\right), \quad (21)$$

where \tilde{N} is a normalization factor, ω_0 is the mean frequency and σ_ω is the spectral width of the wave packet.

Figure 5 demonstrates the tunneling process through a symmetrically placed barrier in the wave guide for an incoming mode of the type \mathbf{H}_{10} . Most of the frequencies in the spectrum (21) are taken above the cutoff frequency ω'_c of the barrier region $L > z > 0$. Correspondingly, the transmission rate is high. We observe that the shape of the reflected and transmitted wave packets is substantially deformed. Among other reasons this is due to the energy transfer to higher modes other than the incoming

mode \mathbf{H}_{10} . In terms of the evolution of the wave-packet maxima, we start with a single maximum in the incoming wave and end up with many transmitted maxima propagating with different velocities in the wave guide.

In Fig. 6 the resonant tunneling of a Gaussian wave packet is shown. The frequency spectrum contains many transmission resonances (see also Fig. 4) leading to multiple reflections of the wave packet at the barrier walls.

In Fig. 7 we compute the longitudinal energy density $\mathcal{W}(z, t)$ in the time domain at a fixed position z behind the barrier and for different barrier lengths L . The wave packet was chosen such that tunneling takes place mainly in the evanescent regime. Under this condition we observe that the maximum of the wave packet can appear behind the barrier earlier than when moving in the free space with the vacuum speed of light c . This behavior becomes more obvious for large L as the transmission rate decreases significantly.

As another example we consider the tunneling of Kaiser–Bessel wave packets [16] with a limited and discrete frequency spectrum in a given interval $[\omega_-, \omega_+]$. The spectral distribution is given by

$$f(n) = \frac{I_0 \left[\pi \alpha \sqrt{1 - (2n/N)^2} \right]}{I_0(\pi \alpha)}, \quad 0 \leq |n| \leq \frac{N}{2}, \quad (22)$$

where α is the parameter characterizing the width of the distribution and N is the number of the stationary-wave components with frequencies $\omega_n = \omega_- + (n + \frac{N}{2})(\omega_+ - \omega_-)/N$ for $n = -N/2, \dots, -1, 0, 1, \dots, N/2$. The distribution (22) ensures optimality of the wave-packet localization in the time domain and was also used in the microwave experiments [1]. In Fig. 8 we compute the tunneling time of the maximum of a Kaiser–Bessel wave packet between the beginning and end of the barrier as a function of the barrier length L . We consider wave packets tunneling in the propagating and evanescent regime and compare in the respective case the tunneling velocity of the maximum with the group velocity in the wave guide and the velocity of light in vacuum c . In the evanescent case we observe the tunneling velocity of the maximum of the wave packet for long barriers to be independent of the barrier length L . This behavior corresponds to the Hartman effect which is well-known from the quantum-mechanical tunneling [17,18]. Thus, evanescent tunneling of the maximum becomes highly superluminal. In the example of Fig. 8 we obtain a tunneling time $\tau_T \approx 127.78$ ps at a barrier length $L = 100$ mm for the maximum of the wave packet. The corresponding tunneling velocity is $v_T = L/\tau_T \approx 2.6c$ in very good agreement with the experimental result given in [1].

IV. QUANTILE MOTION OF ELECTROMAGNETIC SIGNALS. CAUSALITY OF SIGNAL PROPAGATION

We measure the arrival time of a signal with a detector placed at the fixed position z_P . We assume that the region in which the energy of an electromagnetic pulse is essentially different from zero is initially far away from the position z_P of the detector. The detection of the electromagnetic signal requires the deposition of a certain amount W of energy in the detector to cause a change of its state indicating the arrival of the signal. This is equivalent to the condition

$$\int_{z_P}^{\infty} dz \mathcal{W}(z, t) = W \quad (23)$$

on the time t of arrival of the signal. Repeated measurements at different positions z_{P1}, z_{P2}, \dots yield arrival times t_1, t_2, \dots corresponding to these positions. They are discrete points on the trajectory $z_P = z_P(t)$ defined by requiring the condition

$$\int_{z_P(t)}^{\infty} dz \mathcal{W}(z, t) = W \quad (24)$$

to hold at all times t . If we call W_0 the total energy contained in the pulse then $P = W/W_0$ is the fraction of energy needed for detection and $\varrho(z, t) = \mathcal{W}(z, t)/W_0$ is the normalized energy density. Equation (24) can be put into the form

$$\int_{z_P(t)}^{\infty} dz \varrho(z, t) = P, \quad 0 < P < 1 \quad (25)$$

which is the same as Equation (11) of [5]. Therefore, $z_P = z_P(t)$ is the quantile trajectory of the electromagnetic signal. As to be expected it depends on the fraction P , and thus on the sensitivity $W = PW_0$ of the detector. The signal velocity is then given by

$$v_P(t) = \frac{dz_P(t)}{dt}. \quad (26)$$

Examples of quantile trajectories for tunneling Gaussian signals in wave guides of varying cross section are given in Fig. VI and Fig. VI. Figure VI shows that the presence of a barrier in the wave guide may only lead to a slower signal propagation at any give time t and for every detector sensitivity P . Thus, no quantile signal velocity larger than the speed of light in vacuum c is possible. Especially, in the evanescent tunneling regime (see Fig. VIc) the tunneling velocity is much smaller than c , whereas, as physically expected, most of the trajectories turn back to the reflection region.

The behavior of the quantile trajectories for different P values reflects several properties of the tunneling process. In Fig. VIb the reflected and transmitted quantile trajectories split into trajectory bunches propagating with

different velocities in the wave guide. They correspond to the electromagnetic modes produced in the tunneling as described in the previous section. This coincidence between the behavior of quantile trajectories and typical wave phenomena in tunneling can be observed also in resonant tunneling (see Fig. VI).

The causality of quantile motion can explicitly be derived, for instance, in the case of tunneling TE -waves. Using the definition (24) and the continuity relation (15) we derive the quantile velocity (24), c.f. Equation (13) in [5],

$$v_P(t) = \frac{dz_q(t)}{dt} = \frac{\mathcal{S}[z_P(t), t]}{\mathcal{W}[z_P(t), t]}. \quad (27)$$

Trajectories solving this equation have also been studied by Holland [19]. The modulus of the velocity field characterizing the differential equation (27) is

$$|v(z, t)| = \frac{2c \left| \sum_{n=1}^{\infty} \operatorname{Re}[cE_y^n] \operatorname{Re}[H_x^n] \right|}{\left| \sum_{n=1}^{\infty} \operatorname{Re}[cE_y^n]^2 + \operatorname{Re}[H_x^n]^2 + \operatorname{Re}[H_z^n]^2 \right|} \leq c, \quad (28)$$

Thus, $v_q(t)$ never exceeds the vacuum speed of light c , i.e., the signal propagation described by the quantile trajectory is causal. This result is a general property of the quantile motion and holds independently of the type of the tunneling wave.

V. NOTE ON THE QUANTILE MOTION IN DISPERSIVE AND ABSORPTIVE MEDIA

It has been known for a long time that electromagnetic signal propagation in the spectral region of a dispersive medium characterized by anomalous dispersion and strong absorption leads to superluminal phase and group velocity [20–23]. Even though the shape of the propagating signal may be substantially deformed in comparison to the shape of the incoming wave, a propagation velocity has been considered which coincides with the velocity of one of the pulse maxima. Then the velocity obtained this way is again superluminal [23]. This result was recently reconfirmed by the photon experiments at Berkeley [24,25] and by the experiments with photonic barriers in wave guides [26]. However, if one considers instead of the pulse maxima the energy transport in the medium no superluminal velocities occur. Diener [10] suggests a procedure for separating propagating and non-propagating parts of energy of the electromagnetic pulse and obtains subluminal velocities for the energy transport in the medium.

Because of the interaction of the electromagnetic field with the dispersive medium, energy is permanently transferred between the propagating pulse and the oscillating charges in the medium. In the presence of dissipation this

exchange is characterized by a loss of energy, since part of the mechanical energy of the oscillators is steadily transformed into heat. Thus, three different kinds of energy have to be considered, the electromagnetic energy of the pulse, the mechanical energy of the oscillating charges of the medium, and the thermal energy stored in the medium [27]. Each of them may be considered as the energy of an open subsystem of the closed system characterized by the total energy which is conserved.

We apply the concept of quantile motion to the wave propagation in dispersive media. Sufficient condition for this is the existence of a measurable quantity with a positive spatial density (see [5–7]). Since the total energy in the medium is conserved, its density fulfills a continuity equation similar to (14). Thus, quantile trajectories for the total energy in a dispersive and absorptive medium may be easily defined in complete analogy to the above description for the (conserved) electromagnetic energy in wave guides. The application of quantile motion for the electromagnetic signal propagation in dispersive media has been carried through in [27]. In all cases it has been shown that the quantile velocities for the signal remain below the vacuum speed of light c . An argument analogous to the one leading to (28) shows rigorously that the quantile velocity in the oscillator model of dispersive and absorptive media is always smaller than the vacuum speed of light. This and related results will be presented in a forthcoming publication.

VI. CONCLUDING REMARKS

The concept of quantile motion has been applied to the propagation of electromagnetic waves in wave guides of varying cross section and in dispersive and absorptive media. It has been shown that the signal velocity measured with a detector of finite sensitivity never becomes superluminal. In the context of the propagation of electromagnetic signals the quantile velocity is a generalization to detectors with finite sensitivity of Sommerfeld's concept [20] of a front velocity describing the speed of a signal measured with a detector of infinite sensitivity.

-
- [1] A. Enders, G. Nimtz, *J. Phys. I France* **2**, 1693 (1992).
 - [2] A. Enders, G. Nimtz, *J. Phys. I France* **2**, 1089 (1993).
 - [3] A. Enders, G. Nimtz, H. Spieker, *J. Phys. I France* **4**, 565 (1994).
 - [4] A. Enders, G. Nimtz, *Phys. Rev. E* **Vol. 48**, 632 (1993). G. Nimtz, *Superluminal signal velocity*, Talk presented in the Workshop “*Superluminal(?) Velocities*”.
 - [5] S. Brandt, H.D. Dahmen, E. Gjonaj, T. Stroh, *Quan-*

- tile motion*, Talk presented in the Workshop “*Superluminal(?) Velocities*”.
- [6] S. Brandt, H.D. Dahmen, E. Gjonaj, T. Stroh, *Quantile Motion and Tunneling*, Prep. University of Siegen, Germany, SI 95-1.
 - [7] S. Brandt, H. D. Dahmen, E. Gjonaj, T. Stroh, to be published in *Phys. Lett. A*, (1998).
 - [8] P. Thoma, Th. Weiland, *Phys. Bl.* **50 Nr. 4**, 313 (1994).
 - [9] G. Raithel, *Phys. Bl.* **50 Nr. 12**, 1149-1152 (1994).
 - [10] G. Diener, *Phys. Lett. A* **235**, 118-124 (1997).
G. Diener, *Energy transport velocity in dispersive media and devices*, Talk presented in the Workshop “*Superluminal(?) Velocities*”.
 - [11] H. Goenner, *Einstein causality and the superluminal velocities of the Cologne microwave experiments*, Talk presented in the Workshop “*Superluminal(?) Velocities*”.
 - [12] F.E. Borgnis, C.H. Papas, *Randwertprobleme der Mikrowellenphysik*, Springer-Verlag, Berlin, Göttingen, Heidelberg (1955).
 - [13] J.D. Jackson, *Classical Electrodynamics*, John Wiley & Sons, Inc., New York, London, Sydney, Toronto, 2nd ed., (1974).
 - [14] D.J. Bouwkamp, *Physica XII No. 7*, 467 (1946).
 - [15] T. Martin, R. Landauer, *Phys. Rev. A* **45**, 2611 (1992).
 - [16] F.J. Harris, *Proc. IEEE Vol. 66 No. 1*, 51 (1978).
 - [17] T.E. Hartman, *J. Appl. Phys.* **33**, 3427 (1962).
 - [18] E.H. Hauge and J.A. Støvneng, *Rev. Mod. Phys.* **61**, 917 (1989).
C.R. Leavens, in *Tunneling and its Implications*, D. Mugnai, A. Ranfagni and L.S. Schulman (eds.), World Scientific, Singapore, 1997.
 - [19] P.R. Holland, *Phys. Rep.* **224**, 95 (1993).
 - [20] A. Sommerfeld, *Phys. Zeitschr.* **8**, 841 (1907).
 - [21] A. Sommerfeld, *Ann. der Phys.* **44**, 177-201 (1914).
 - [22] L. Brillouin, *Wave Propagation and Group Velocity*, Academic Press N.Y., (1960).
 - [23] E. Gjonaj, *Wave packet motion and speed of the signal in the resonance frequency region of dispersive media*, Diploma work, University of Siegen, Germany, (1993).
 - [24] A.M. Steinberg, R.Y. Chiao, *Phys. Rev. A* **49**, 2071 (1994).
 - [25] A.M. Steinberg, P.G. Kwiat, R.Y. Chiao, *Phys. Rev. Lett.* **71**, 708-711 (1993).
A.M. Steinberg, *Causal nonlocality in tunneling: can a tunneling tree make a noise in two forests at the same time*, Talk presented in the Workshop “*Superluminal(?) Velocities*”.
 - [26] G. Nimtz, H. Spieker, H.M. Brodowsky, *J. Phys. I France* **4**, 1379-1382 (1994).
 - [27] E. Gjonaj, *Quantilbewegung und Kausalität*, Ph.D. Thesis, University of Siegen, Germany, (1998).

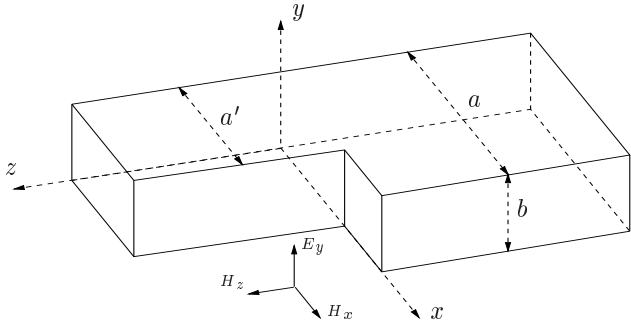


FIG. 1. Geometry of a wave guide with a reduction of the cross section beginning at $z = 0$ and extending to infinity. This configuration with an \mathbf{H}_{n0} wave incident from the right corresponds to a quantum-mechanical potential step.

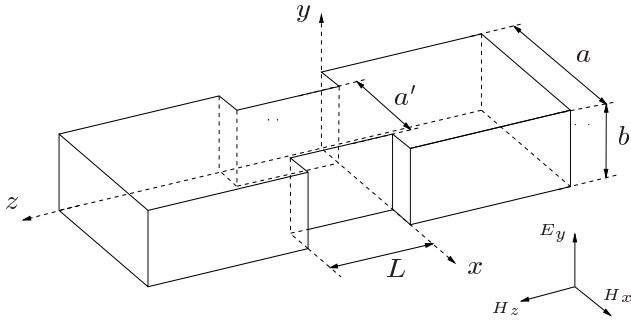


FIG. 2. Geometry of a wave guide with a symmetric reduction of the cross section between $z = 0$ and $z = L$ corresponding to a barrier of finite length L .

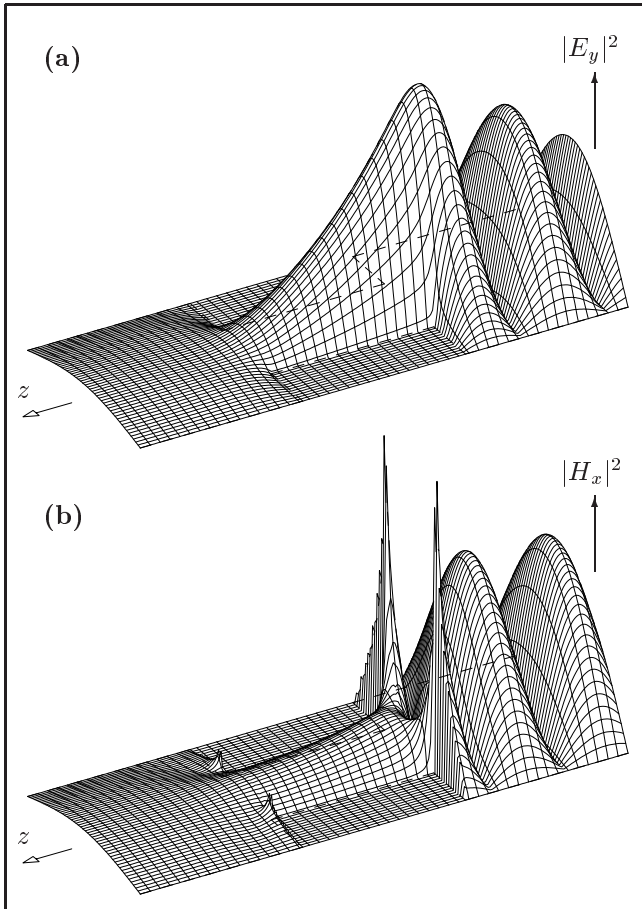


FIG. 3. Stationary fields in evanescent tunneling. The dimensions of the symmetric wave guide and of the barrier are $a = 1$ cm, $a' = 0.4$ cm, and $L = 1$ cm (see Fig. VI). The incoming wave incident from the right is an \mathbf{H}_{10} mode of frequency $\omega = 21$ GHz. (a) The electric field strength $|E_y|^2$ is shown. This component is continuous everywhere and vanishes at the walls of the wave guide. (b) The transverse magnetic field strength $|H_x|^2$ is shown. Obviously, the magnetic field is singular at the edges at $z = 0$ and $z = L$ of the wave guide.

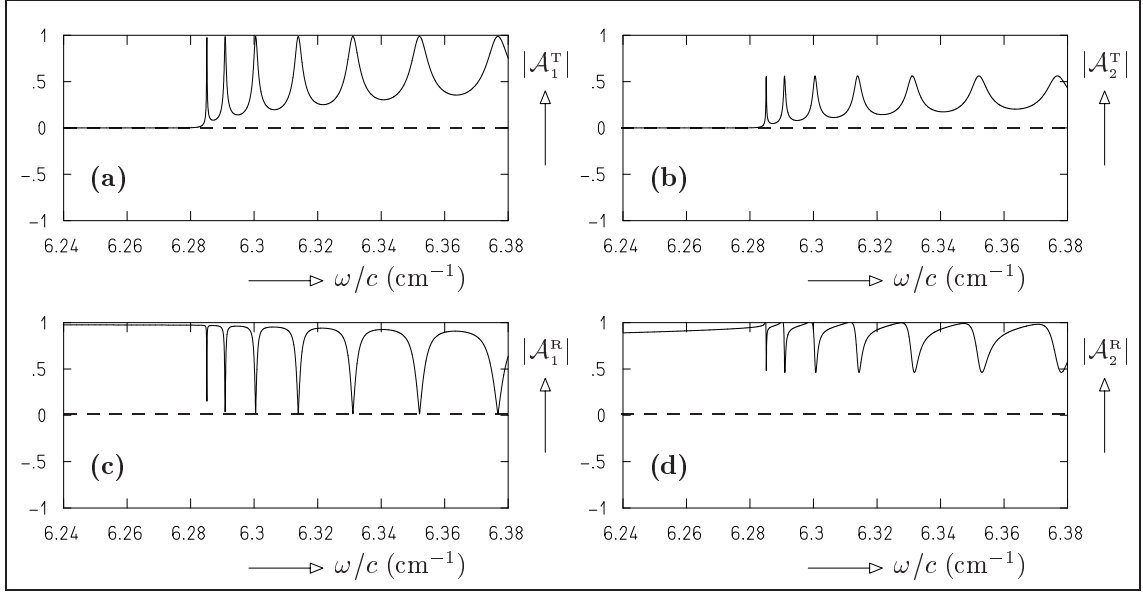


FIG. 4. Spectral diagram with the transmission and reflection coefficients of the first first two modes \mathbf{H}_{10} and \mathbf{H}_{20} , where \mathbf{H}_{10} is the incident mode. The dimensions of the wave guide and of the symmetric barrier are $a = 1$ cm, $a' = 0.5$ cm, and $L = 1$ cm (see Fig. VI).

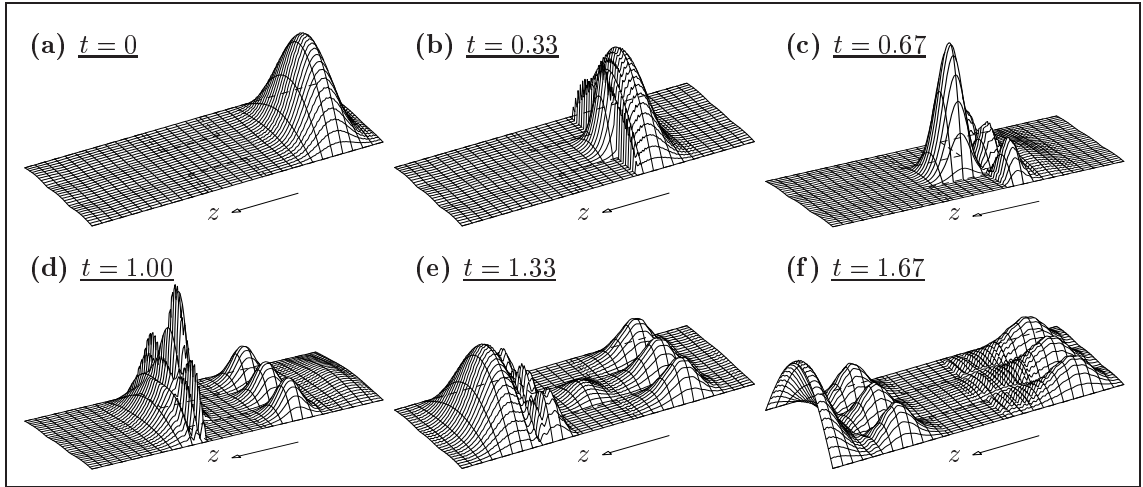


FIG. 5. Time development of a tunneling Gaussian wave packet. The electric field strength $|E_y|^2$ is shown. The dimensions of the wave guide are $a = 1$ cm, $a' = 0.5$ cm, and $L = 5$ cm. The incident wave packet is of the type \mathbf{H}_{10} with frequencies centered at $\omega_0 = 30$ GHz and spectral width $\sigma_\omega = 1.5$ GHz. The production of higher modes in tunneling which propagate with different velocities in the wave guide, is observed. Times are given in picoseconds.

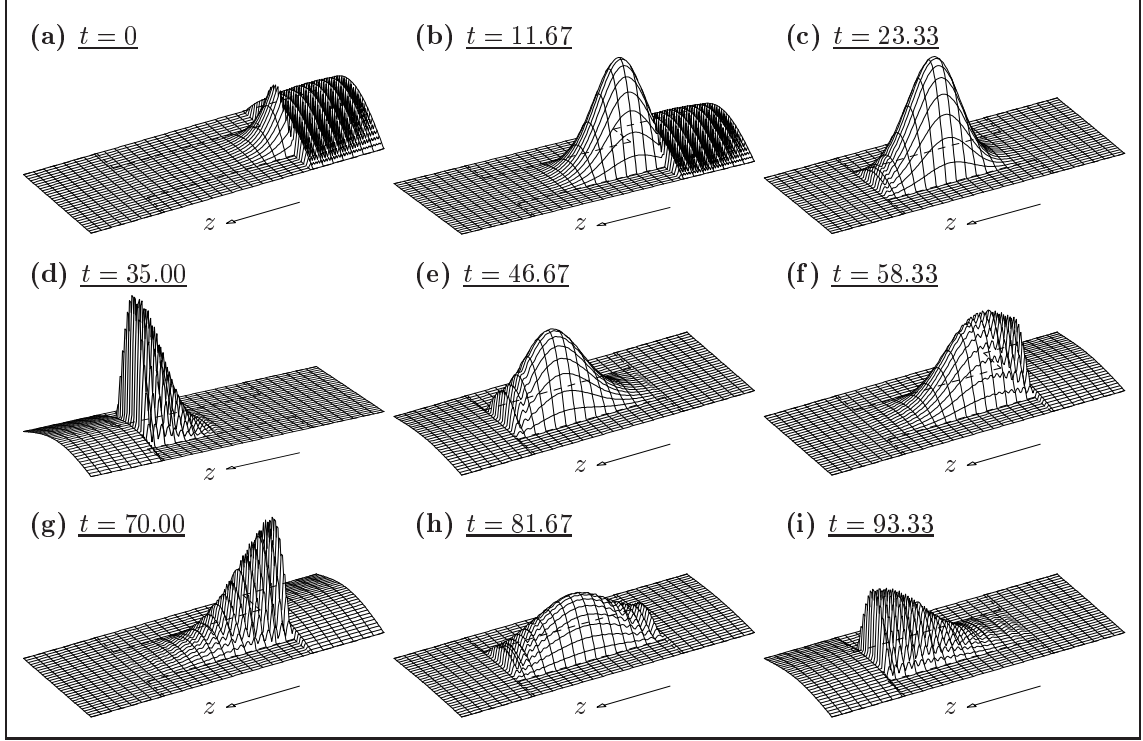


FIG. 6. Time development of a tunneling Gaussian wave packet in resonant tunneling. The electric field strength $|E_y|^2$ is shown. The dimensions of the wave guide are the same as in Fig. 4. The spectral function of the incoming wave packet centered at $\omega_0 = 18.97$ GHz with $\sigma_\omega = 0.015$ GHz extends over more than one resonance (see Fig. 4), so that multiple reflection inside the barrier is observed. Times are given in picoseconds.

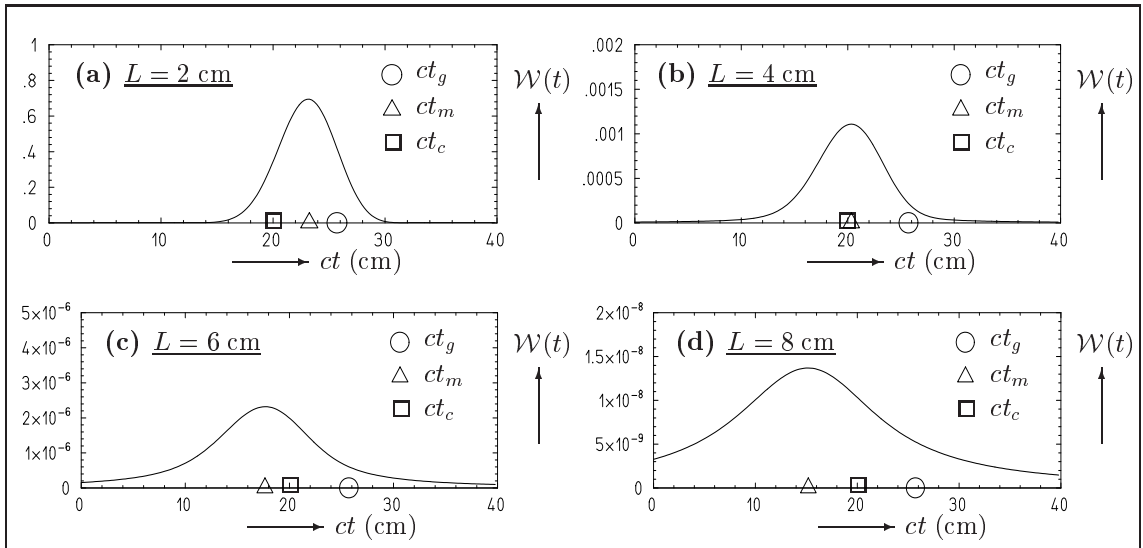


FIG. 7. Example of the superluminal tunneling of the maximum of a tunneling Gaussian wave packet. The longitudinal energy density $\mathcal{W}(z, t)$ is shown in the time domain at a fixed position behind the barrier $\Delta z = 20$ cm away from the position of the center of the wave packet at $t = 0$. The dimensions of the symmetric wave guide are $a = 1$ cm and $a' = 0.5$ cm for different barrier lengths L (see Fig. VI). The incident wave packet is of the type \mathbf{H}_{10} with frequencies centered at $\omega_0 = 15$ GHz and spectral width $\sigma_\omega = 0.6$ GHz. Thus, evanescent tunneling occurs. The box, the triangle, and the circle correspond to the arrival times of the pulse maximum in vacuum, in a wave guide without barrier, and in the wave guide with a barrier of length L , respectively. If the barrier is long enough the tunneling velocity of the pulse maximum becomes superluminal (case (c) and (d)).

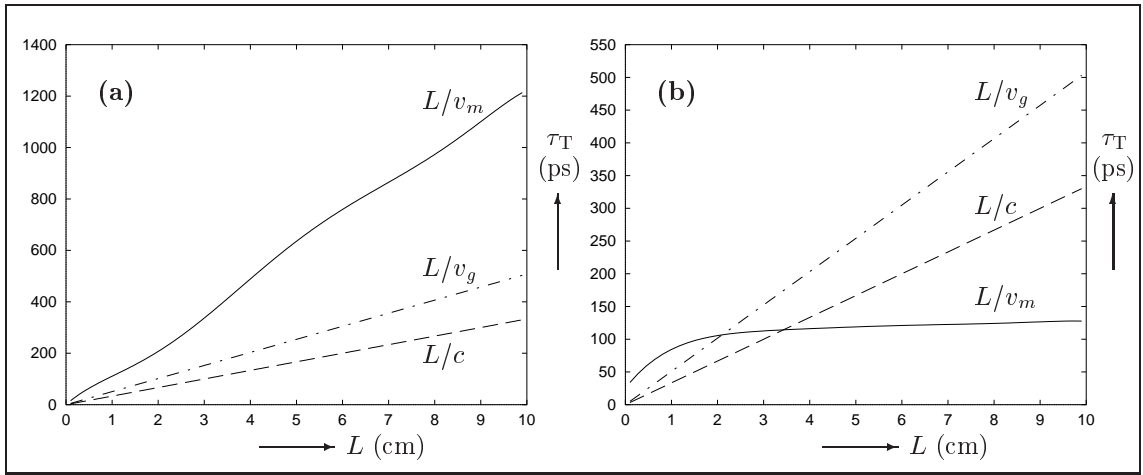


FIG. 8. Tunneling times of the pulse maximum and Hartman effect. The transmission time of the pulse maximum (solid line), the time intervals corresponding to the free motion of the pulse maximum in vacuum (dashed line) and in the wave guide without barrier (broken line) for a Kaiser–Bessel wave packet are plotted as functions of the barrier length L . In both cases the incoming wave packet is a superposition of $N = 800$ frequencies in the interval $51.52 \text{ GHz} \leq \omega \leq 57.81 \text{ GHz}$ with the spectral distribution (22) for $\alpha = 1$. **(a)** Non-evanescent tunneling. The cross sections of the wave guide are $a = 22.86$ mm and $a' = 18$ mm. The behavior of the tunneling times is “normal”. **(b)** Evanescent tunneling. Here, the same tunneling situation as in [1] is computed, i.e., the two cross sections of the wave guide are $a = 22.86$ mm and $a' = 15.8$ mm. The transmission time $\tau_T = L/v_m$ for long barriers remains nearly constant and, thus, implies superluminal tunneling for the pulse maximum.

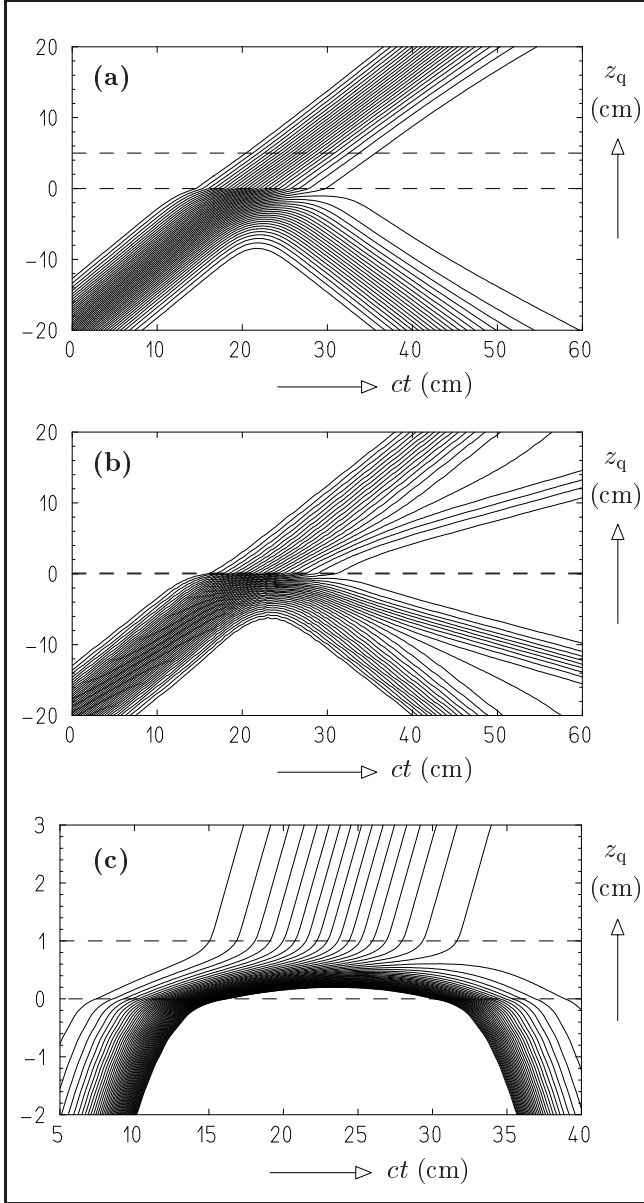


FIG. 9. Quantile trajectories. **(a)** Non-evaescent tunneling. Trajectories for $0.05 \leq P \leq 0.95$ in steps of $\Delta P = 0.02$ are shown. The dimensions of the symmetric wave guide (see Fig. VI) are $a = 1$ cm, $a' = 0.3$ cm, and $L = 5$ cm. The incoming Gaussian wave packet is of the type \mathbf{H}_{10} with $\omega_0 = 60$ GHz and $\sigma_\omega = 0.3$ GHz. **(b)** Evanescent tunneling with short barrier. The cross sections a and a' are the same as in **(a)**. The length of the barrier is $L = 0.1$ cm. The incoming wave packet with $\omega_0 = 30$ GHz and $\sigma_\omega = 0.3$ GHz is evanescent in the region inside the barrier. **(c)** Evanescent tunneling with long barrier. The length of the barrier is chosen to $L = 1$ cm. The incoming wave packet has $\omega_0 = 22.5$ GHz and $\sigma_\omega = 0.3$ GHz. Because of the strong reflection, trajectories for $10^{-3} \leq P \leq 2.5 \times 10^{-2}$ in steps of $\Delta P = 5 \times 10^{-4}$ are computed. Also in this case no superluminal tunneling is observed.

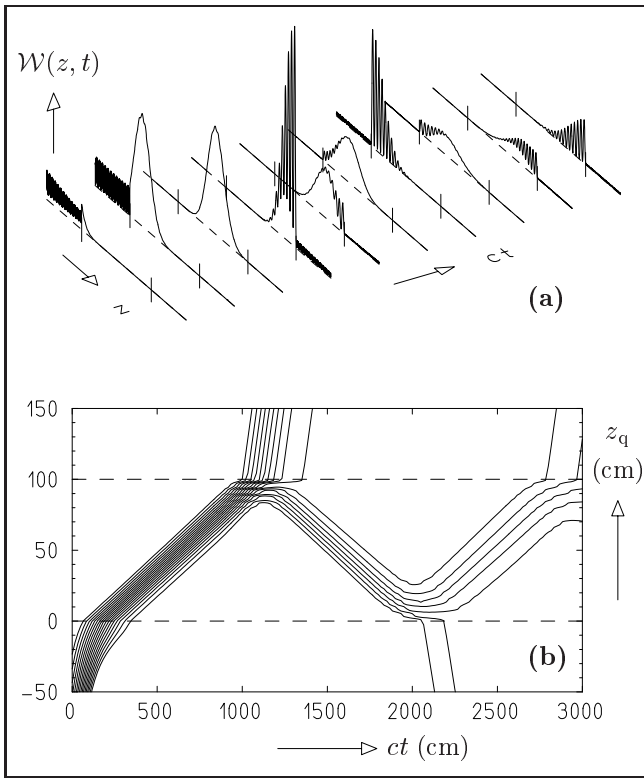


FIG. 10. Quantile trajectories in resonant tunneling. The dimensions of the symmetric wave guide are $a = 1$ cm, $a' = 0.5$ cm, and $L = 100$ cm. The incoming wave is a Gaussian wave packet of the type \mathbf{H}_{10} with $\omega_0 = 18.97$ GHz and $\sigma_\omega = 0.015$ GHz. (a) Time development of the longitudinal energy density $\mathcal{W}(z, t)$. (b) Quantile trajectories for $0.2 \leq P \leq 0.625$ in steps of $\Delta P = 0.025$. The oscillating behavior of the quantile trajectories reflects the time development shown in (a).